RSC Advances

PAPER

Cite this: *RSC Adv.*, 2022, **12**, 4162

Low-temperature thermal conversion of Al-substituted goethite in gibbsitic bauxite for maximum alumina extraction

Guotao Zhou, Yilin Wang,* Tiangui Qi, Qiusheng Zhou, Guihua Liu, Zhihong Peng and Xiaobin Li*

The conversion of Al-substituted goethite (Al-goethite) to hematite in gibbsitic bauxite is conducive to alumina extraction during the Bayer process and the enrichment of iron minerals in red mud. In this work, mineralogical characteristics of gibbsitic bauxite were identified by AMICS analysis, and the low-temperature thermal conversion behavior of both synthetic Al-goethite and natural Al-goethite in gibbsitic bauxite were investigated through thermal gravity analysis, phase transformation, and microstructure studies. Results show that the proportion of aluminum in Al-goethite reached 12.68% of the total aluminum content in gibbsitic bauxite. The conversion of synthetic Al-goethite to hematite starts at ~280 °C, while that of natural Al-goethite starts at ~320 °C, and the addition of NaOH can accelerate the conversion. The formed hematite inherits the needle-like appearance of the original Al-goethite, has many holes on the surface due to dehydroxylation, and no migration of aluminum elements occurs during the roasting process, indicating that Al-goethite transformed into porous Al-substituted hematite (Al-hematite), which is beneficial to the extraction of the aluminum retained in the hematite structure during Bayer digestion. To confirm the above results, digestion experiments (without or with roasting for typical Bayer digestion or low-temperature roasting-Bayer digestion) were carried out with gibbsitic bauxite and the one roasted at 400 °C for 30 min as raw materials, respectively. Compared to the typical Bayer digestion, the relative alumina recovery of low-temperature roasting-Bayer digestion increased from 90.06% to 95.65%, the red mud yield decreased from 36.32% to 34.08%, and the grade of Fe in red mud increased from 48.45% to 52.88% at 270 °C for 60 min. Enhanced transformation of Al-goethite significantly improves alumina recovery and the resultant iron-rich red mud can be easily co-processed in the steel industry, thus significant emission reduction of red mud from the Bayer system might be achieved.

Received 13th December 2021
Accepted 24th January 2022

DOI: 10.1039/d1ra09013e

rsc.li/rsc-advances

1. Introduction

The high-iron gibbsitic bauxite in the Boké region of Guinea has become an important raw material for the global alumina industry.[1] Generally, gibbsitic bauxite contains an appreciable amount of Al-goethite,[2,3] causing alumina loss due to the isomorphous substitution of aluminum in place of the Fe atoms with a maximum of 33 mol% in the goethite lattice.[4,5] Furthermore, the sedimentability, filterability, and washability of the formed red mud slurry deteriorate owing to the non-compact crystal structure of goethite.[6–8] The conversion of Al-goethite is of great significance to the efficient utilization of gibbsitic bauxite and has therefore received great attention. Currently, a wide variety of processes have been proposed for the conversion of Al-goethite and can be categorized into hydrometallurgy and pyrometallurgy.

In the hydrometallurgical process (mainly referring to the Bayer process), the conversion of Al-goethite can be promoted by increasing the Bayer digestion temperature and the caustic concentration,[9,10] but in the commonly adopted digestion temperature range (<280 °C) and caustic concentration (<240 g L^{-1}), the complete conversion of Al-goethite is still difficult. The addition of lime or calcium-containing additives can improve the hydrothermal conversion,[11–14] but excessive lime addition is necessary for the industrial digestion process, leading to detrimental consequences for alumina recovery, the discharge of red mud, and the iron mineral sorting performance.[15,16] The addition of reducing agents, such as saccharide,[17] iron powder,[18] and glycerol,[19] can also promote the conversion of Al-goethite to hematite or magnetite. However, the use of a large amount of reducing agent greatly affects the balance of organic matter in the Bayer digestion system, which needs further optimization.

School of Metallurgy and Environment, Central South University, No. 932, Lushan Road, Changsha 410083, Hunan, China. E-mail: wang.yi.lin@outlook.com; x.b.li@csu.edu.cn; Fax: +86 731 88830453

In pyrometallurgical methods, the conversion of goethite or Al-goethite usually refers to dehydration conversion due to the temperature increase during heating or mechanical grinding.[20,21] A general agreement exists on the fact that the temperature of thermal conversion increases with the Al substitution in Al-goethite.[22] With the Al substitution for Fe of up to 14 mol%, the conversion temperature range of Al-goethite shifted to 247–320 °C.[23] In addition, the difficulty of converting Al-goethite increases with the crystallinity of Al-goethite, and the conversion temperature can increase from 260 °C to 320 °C.[24–26] However, the mechanism of thermal conversion of Al-goethite has two points. Wolska used X-ray diffraction (XRD) and infrared spectroscopy (IR) to observe that intermediate structures referred to as "proto-hematite" and/or "hydro-hematite" were formed by the dehydration of goethite in the temperature range of 180–250 °C and completely transformed into hematite at 800–1050 °C.[27] Other researchers insist that the process is a direct conversion from goethite to hematite and does not form any intermediate.[28,29] The addition of reducing agents during the thermal conversion process to induce the conversion of goethite and Al-goethite to magnetite has also been widely reported, with the conversion temperature varying depending on the type of reducing agents.[30–32] Processing goethite-rich iron ores using reduction roasting followed by low-intensity magnetic separation can obtain an iron concentrate with a total iron grade of ~66.6% and iron recovery of ~90.4% at 800 °C for 30 min using 10% coal.[33] According to the literature,[34] a good temperature for converting goethite to magnetite through reduction roasting was found to be between 650 °C and 700 °C in 50%/50% CO/CO_2 mixtures. Furthermore, the reduction of goethite ore with carbohydrates starts at ~450 °C, with the maximum at ~520 °C.[35] However, the thermal conversion process of Al-goethite still faces the problems of high energy consumption and high cost. Moreover, no report has been published on the mechanism of the conversion of Al-goethite in bauxite at low-temperature roasting and the digestion performance in the Bayer process.

In this work, the distribution characteristics of Al-goethite in gibbsitic bauxite in the Boké region of Guinea were first identified by the advanced mineral identification and characterization system (AMICS). Then, the thermal conversion behavior of both synthetic Al-goethite and natural Al-goethite in gibbsitic bauxite at temperatures between 200 °C and 400 °C were investigated through thermal gravity analysis, phase transformation, and microstructure. The effect of NaOH on the roasting process was also studied. Finally, the effect of the low-temperature roasting process on Bayer digestion (relative alumina recovery, degree of iron enrichment, and organic matter content of the digestion Bayer liquid) was clarified. The results of this study can help in the better understanding of the phase structure changes of Al-goethite during the roasting process and provide a theoretical basis for the efficient conversion of Al-goethite to hematite in gibbsitic bauxite.

2. Experimental

2.1 Materials

The $Fe(NO_3)_3 \cdot 9H_2O$, $Al(NO_3)_3 \cdot 9H_2O$, KOH, NaOH, and $Al(OH)_3$ were of analytical grade (>99%) and purchased from Shanghai Macklin Biochemical Co., Ltd in China. The preparation of synthetic Al-goethite was based on a previous report.[36] Briefly, $Fe(NO_3)_3 \cdot 9H_2O$ and $Al(NO_3)_3 \cdot 9H_2O$ were dissolved in 400 mL of deionized water by continuous stirring to form a transparent yellow solution. Subsequently, 5 and 0.5 mol L^{-1} KOH solutions were used to adjust the pH to 12.5 ± 0.1. The suspensions were stirred for 60 min and then aged for 14 days at 70 °C. The final product was washed with deionized water. Finally, the samples were dried in an oven at 50 °C for 24 h and then cooled to room temperature for further use. The SEM image and XRD pattern of the synthetic Al-goethite particles are shown in Fig. 1. From Fig. 1(a), the SEM image of synthetic samples shows typical acicular and rod-like morphologies, which is consistent with the literature report of goethite morphology,[37] suggesting that the synthetic samples may be goethite. In addition, the XRD patterns in Fig. 1(b) indicate that the characteristic peaks of the synthetic samples matched well with the standard card of goethite [JCPDS (29-0713)], revealing that goethite nanoparticles were successfully synthesized. The composition of synthetic samples was analyzed by using an inductively coupled plasma emission spectrometer (ICP-OES), and the results show an alumina content of 3.05%, a ferric oxide content of 85.84%, and the Al/(Fe + Al) molar ratio of 5.27, implying that 5.27 mol% aluminum was built into the goethite lattice in place of Fe

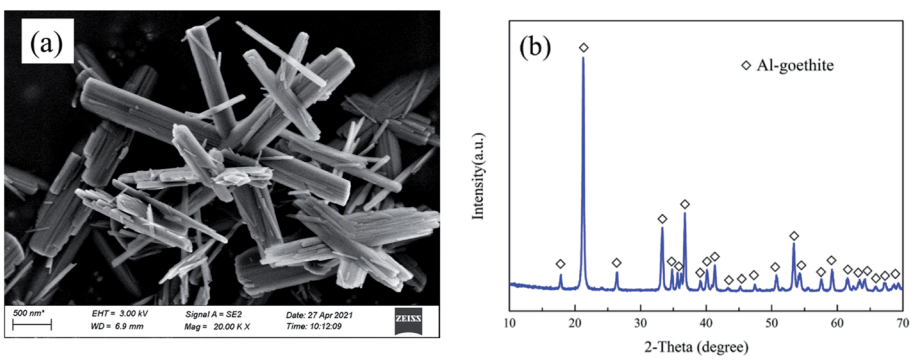

Fig. 1 Characteristics of synthetic Al-goethite: (a) SEM image and (b) XRD patterns.

atoms, forming Al-goethite with the formula $Fe_{0.9473}Al_{0.0527}OOH$.

The Al-goethite containing gibbsitic bauxite was obtained from Boké region of Guinea, and its composition was analyzed by ICP-OES. The results indicate that the alumina, silicon dioxide content, and ferric oxide were 44.69%, 2.11%, and 25.21%, respectively. In addition, the total organic carbon content was 0.25%. The XRD analysis in Fig. 2 indicates that gibbsite and boehmite are the primary aluminum minerals. The silicate minerals include kaolinite and quartz. Goethite, Al-goethite, and hematite are the main iron minerals. Titanium minerals include anatase and rutile.

The Bayer liquor containing $[Na_2O_k] = 230$ g L^{-1} and $[Al_2O_3] = 126$ g L^{-1} was prepared by dissolving NaOH and $Al(OH)_3$. Na_2O_k denotes the caustic alkali in Na_2O.

2.2 Low-temperature roasting

The synthetic Al-goethite or gibbsitic bauxite was sufficiently mixed with 10% NaOH (mixture). Predetermined 10 g of starting materials, namely, synthetic Al-goethite, gibbsitic bauxite, or mixture, were weighed into a flat bottom crucible before they were placed in a muffle furnace at the desired roasting temperature. The roasting temperature varied between 200 °C and 400 °C, and the roasting time was 30 min. After roasting, the samples were removed from the muffle furnace, cooled in air, and weighed before subsequent analysis. Meanwhile, the quality change and the roasting loss rate of the samples before and after roasting were determined under different conditions.

2.3 The Bayer digestion

The Bayer digestion experiments were carried out in a molten mixed nitrate salt cell (YYL-150ML/6, Dingda Chemical Machinery Co. Ltd, China). Starting materials, namely, 31.25 g bauxite or 24.78 g roasted bauxite (at 400 °C for 30 min, weight loss rate of 79.24% based on LOI analysis), were digested with 100 mL of Bayer liquor in a 150 mL sealed rotating steel reactor immersed in a molten mixed nitrate salt cell at a preset temperature. To enhance stirring, 2 × Φ15 mm and 4 × Φ15 mm steel balls were added into the reactor in advance. After the reaction, the reactors were taken out of the cell and then immediately cooled in tap water. The obtained slurry was subsequently filtered, and the filter cake was washed with hot water and then dried at 100 °C for 6 h before analysis.

The relative alumina recovery during Bayer digestion is calculated using eqn (1):

$$\eta(Al_2O_3) = \frac{(A/S)_1 - (A/S)_2}{(A/S)_1 - 1} \times 100\%, \quad (1)$$

where $\eta(Al_2O_3)$ is the relative recovery of alumina, and $(A/S)_1$ and $(A/S)_2$ are the mass ratios of alumina to silica in bauxite and red mud, respectively.

The removal rate of TOC during Bayer digestion is calculated using eqn (2):

$$\eta(TOC) = \left(1 - \frac{V_2 \times \rho_2}{V_1 \times \rho_1}\right) \times 100\%, \quad (2)$$

where V_1 and V_2 represent the volume of Bayer liquid after typical Bayer digestion and low-temperature roasting-Bayer digestion, respectively, and ρ_1 and ρ_2 represent the concentration of TOC Bayer liquid after typical Bayer digestion and low-temperature roasting-Bayer digestion, respectively, at the same digestion temperature.

2.4 Characterization of the samples

All the samples have been dried at 100 °C for 12 h before characterization analysis. Automated quantitative mineralogy analyses were performed on gibbsitic bauxite by AMICS, which consists of a scanning electron microscope (Sigma 300, Carl Zeiss AG, Germany), an energy spectrometer (Quantax 400, Bruker, Germany), and a mineral analysis software (AMICS analysis software, Bruker, Germany). The thermogravimetry and derivative thermal gravimetry curves of samples at the temperature range from 30 °C to 820 °C were determined using a thermal analyzer (STD650, Waters, USA) at the heating rate of 10 °C min^{-1} in an air stream under atmospheric pressure. The mineral phases were characterized by XRD (TTR III, Rigaku, Japan) using Cu Kα radiation at a scan rate of 5° min^{-1}. The microscopic surface morphology and the microscale composition were analyzed through SEM (Zeiss sigma 300, Carl Zeiss AG, Germany; MIRA3-LMH, Tescan, Czech Republic) and X-ray energy spectrometry (SmartEDX, EDAX Inc, USA; EDX-MAX20, Oxford, England). Chemical analysis of the samples was performed *via* fusion method (750 °C for 15 min with a mixture of NaOH followed by direct dissolution in boiling deionized water) through ICP-OES (ICAP7400 Radial, Thermo Fisher Scientific, USA). The organic matter content of the samples was determined by the potassium dichromate capacity external heating method.[38] The total concentration of organic matter in the Bayer liquid was measured using the total organic carbon (TOC-L CPH, Shimadzu (Suzhou) Instruments Manufacturing Co., Ltd, China).

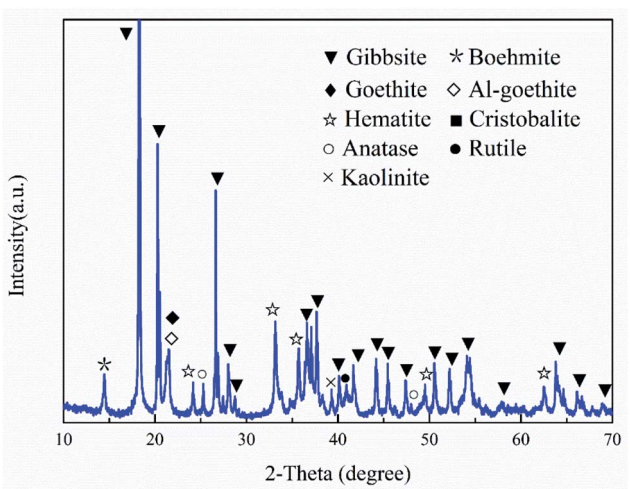

Fig. 2 XRD patterns of gibbsitic bauxite.

3. Results and discussion

3.1 AMICS of gibbsitic bauxite

To illustrate the dissemination characteristics and relations among the minerals, the gibbsitic bauxite was scanned for quantitative image analysis using AMICS, and the results are presented in Fig. 3. The mineral maps in Fig. 3(a) show that gibbsite, boehmite, hematite, goethite, and Al-goethite are irregular granular, plate-like, or elongated and mostly have obvious dissociation characteristics and exist independently. However, there is also intercalation between minerals. From Fig. 3(b), gibbsite occasionally occurs as inclusions within goethite and Al-goethite in the form of aggregates, thus possibly hindering gibbsite digestion during the Bayer process. From Fig. 3(c), the main minerals in bauxite are gibbsite, boehmite, hematite, goethite, and Al-goethite and the proportions of them are 60.06%, 2.74%, 9.35%, 5.05%, and 15.90%, respectively. The minerals in the gibbsitic bauxite compare well with the XRD in Fig. 2 for major minerals but identify a much wider range of minor minerals that were below the detection limit for XRD,

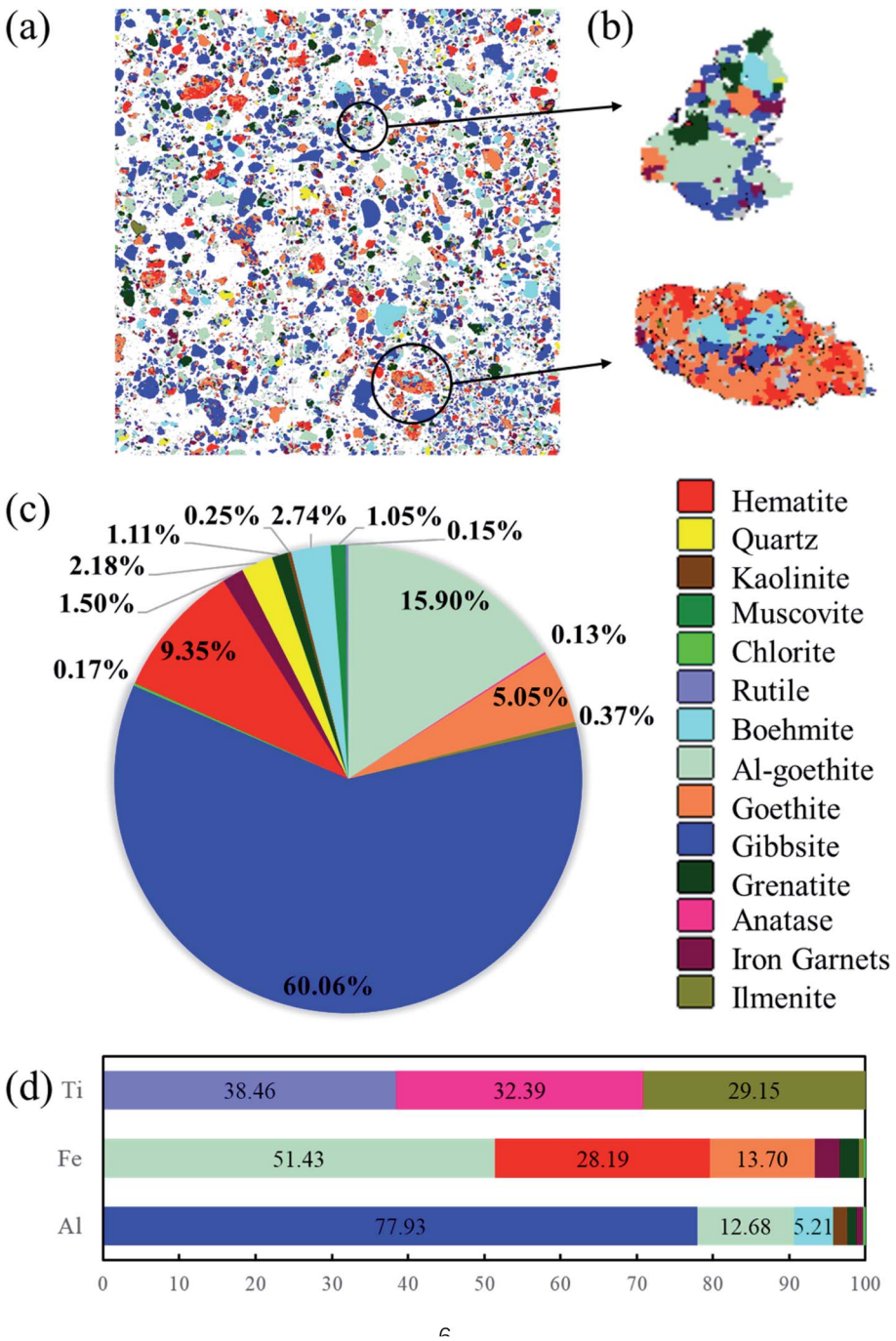

Fig. 3 The AMICS results for gibbsitic bauxite (a) and (b) minerals distribution, (c) minerals proportions, and (d) proportions of Ti, Fe, Al in minerals.

such as ilmenite, chlorite, iron garnet, and muscovite. From Fig. 3(d), the aluminum contents of the gibbsite and boehmite in bauxite account for approximately 77.93% and 5.21%. The main forms of iron minerals are hematite, goethite, and Al-goethite with an iron content of 28.19%, 13.70%, and 51.43% of the iron content in bauxite, respectively, which exist in granular or platelike single-crystal aggregates along with each other. The proportion of aluminum in Al-goethite is up to 12.68% of the aluminum content in bauxite because Al incorporation into the crystal structure of goethite occurs *via* the isomorphous ionic substitution of Al for Fe in goethite formation. The mass distribution data of different sized fractions of gibbsitic bauxite are presented in Fig. 4. As is shown in Fig. 4, the gibbsitic bauxite is a mixture of particles of different sizes, from fine (−2.79 μm) to coarse (−150 μm). The boehmite particles are coarser than those of the gibbsite, and the goethite/Al-goethite particles are also coarser than those of hematite.

3.2 Thermal conversion of synthetic Al-goethite

3.2.1 TG–DSC analysis. To investigate the thermal decomposition conversion of synthetic Al-goethite during low-temperature roasting, the thermal behaviors of synthetic Al-goethite without NaOH and mixed with 10 wt% NaOH were observed through TG–DSC as shown in Fig. 5. As illustrated in Fig. 5(a), the mass loss can be observed in the temperature range 171–336 °C, the weight loss at 820 °C was 10.70%, and the endothermic peak was found at 310 °C and was related to the decomposition of Al-goethite.[39] From Fig. 5(b), the weight loss at 820 °C is 13.63% and the endothermic peak at 303 °C and 589 °C is related to the decomposition of Al-goethite and generation of sodium ferrate,[40] respectively. Compared without the addition of NaOH, the temperature of the endothermic peaks of Al-goethite on the DSC curve with NaOH decreased by 7 °C, implying that NaOH is beneficial to decreasing the conversion temperature of Al-goethite.

3.2.2 Loss on ignition. To determine the change in mass percentage of water resulting from the conversion of Al-goethite, loss on ignition was performed. The effect of the roasting temperature between 200–400 °C on synthetic Al-goethite without NaOH or mixed with 10 wt% NaOH weight loss was investigated, and the related weight loss is displayed in Fig. 6. It can be observed from Fig. 6 that the mass loss of Al-goethite without NaOH or Al-goethite mixed with 10 wt% NaOH increases with the temperature. The mass loss of Al-goethite with the addition of NaOH reached 7.63% at 280 °C, which was higher than the 4.49% mass loss of Al-goethite without NaOH, indicating that the addition of NaOH can promote the conversion of Al-goethite.

3.2.3 XRD analysis. To further understand the phase conversion of Al-goethite by low-temperature roasting, the XRD patterns of roasted products of synthetic Al-goethite without NaOH or mixed with 10 wt% NaOH over temperatures ranging from 200 °C to 400 °C for 30 min are displayed in Fig. 7. Fig. 7(a) shows that Al-goethite remains in the roasted product as the only phase when thermal treatment is performed below 240 °C for 30 min. Conversion has yet to occur at this temperature. As

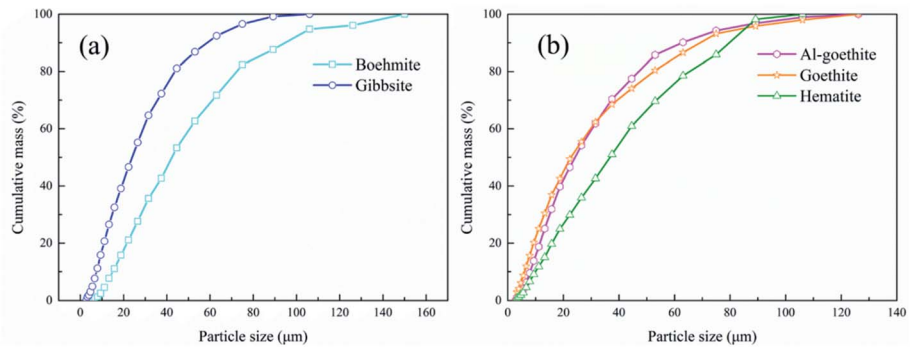

Fig. 4 Main mineral particle size distribution of (a) aluminum minerals and (b) iron minerals.

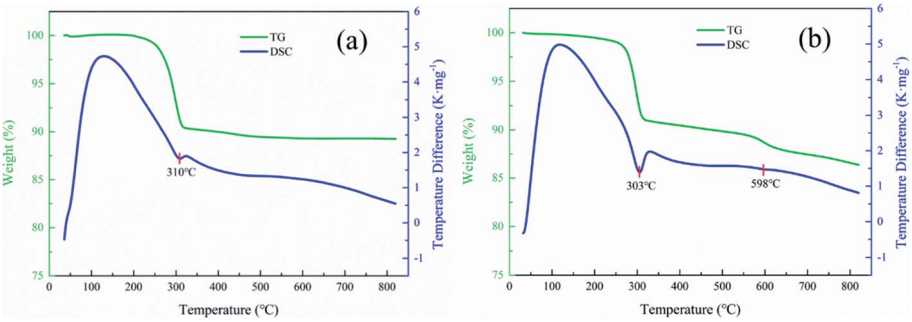

Fig. 5 TG–DSC curves of synthetic Al-goethite (a) without NaOH and (b) mixed with 10 wt% NaOH.

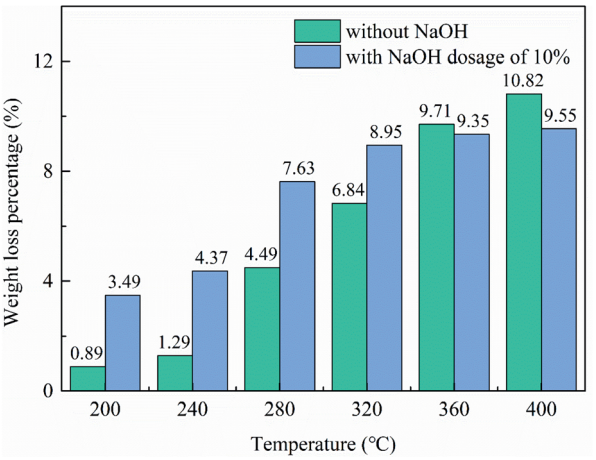

Fig. 6 Effect of roasting temperature on weight loss of synthetic Al-goethite.

the temperature increases to 280 °C, Al-goethite and hematite can be both found in the XRD pattern of the roasted product, suggesting the conversion of Al-goethite to hematite. Further increases in temperature to 320 °C show that hematite is the only phase in the roasted product. The diffraction peak intensity of hematite gradually increases as the temperature continues to rise to 400 °C, indicating that hematite has good crystallinity. Therefore, the XRD patterns indicate that the extent of thermal conversion of Al-goethite to hematite greatly depends on the increase in roasting temperature. As presented in Fig. 7(b), the XRD patterns are similar to the process of roasting Al-goethite without NaOH in the case of adding 10 wt% NaOH. However, as the temperature increases to 280 °C, the diffraction peaks of Al-goethite nearly disappear, and the intensity of the diffraction peaks is lower than that of a roasted product without NaOH at the same temperature. Hematite is the dominant phase in the roasted product, implying that NaOH is beneficial to promoting the conversion of Al-goethite. In addition, the formation of the aluminum phase was not observed in Fig. 7(a), implying that aluminum replaced Fe atoms in the newly formed hematite lattice, thus possibly forming Al-hematite.

3.2.4 SEM analysis. To further comprehend the microstructure conversion process of Al-goethite, the SEM images and EDS mappings for the reaction products roasted at 360 °C for 30 min are displayed in Fig. 8 and 9, respectively. Al-goethite completely transformed to hematite in terms of mineral phase, which can be observed from the XRD results in Fig. 7(a). Fig. 8 displays that this conversion only occurred within the goethite-like structure. In other words, the strains caused by the de-hydroxylation pores during the departure of OH^- are not strong enough to induce the beak-down of the parent goethite crystal. Thus, the thermally treated goethite even at a temperature as high as 360 °C still shows a goethite-like shape with several visible de-hydroxylation pores. Combined with the distribution map of major elements in Fig. 9, findings show that the coincidental distribution of Al, and Fe, which combined with the XRD pattern in Fig. 7(a), confirm the formation of Al-hematite. Remarkably, the surface of the Al-hematite appears the number of pores increases as NaOH is added, indicating that the addition of NaOH can promote the conversion of Al-goethite.

3.3 Thermal conversion of Al-goethite containing gibbsitic bauxite

3.3.1 TG–DSC analysis. To investigate the thermal decomposition behavior of gibbsitic bauxite during low-temperature roasting, the thermal behaviors of gibbsitic bauxite without NaOH and mixed with 10 wt% NaOH were observed through TG–DSC as shown in Fig. 10. The main mass loss processes ended at approximately 700 °C, although a very slow mass loss process continued up to the end of the experiment, the total weight loss at 820 °C was 24.36% and the decomposition of gibbsitic bauxite occurred in three stages. As illustrated in Fig. 10(a), the first mass loss can be observed in the temperature range 180–347 °C and the endothermic peak was found at 302 °C and was likely caused by the decomposition of gibbsite.[41] The second mass loss occurred at 347–410 °C and the endothermic peak at 364 °C was related to the decomposition of

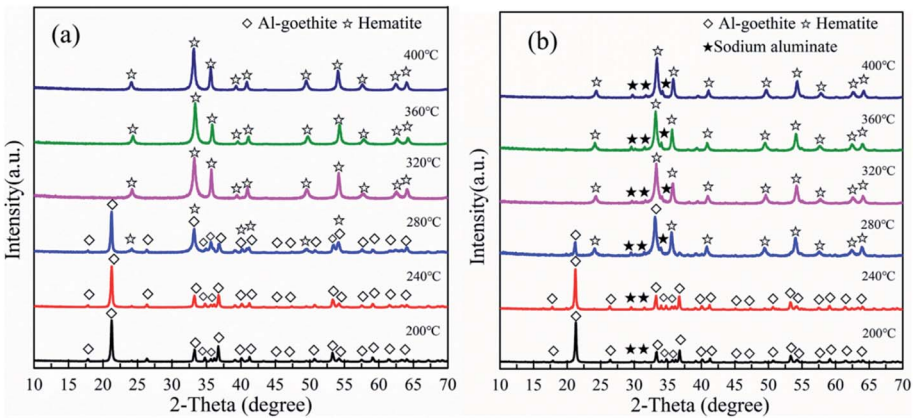

Fig. 7 XRD patterns of roasted products of synthetic Al-goethite at 200–400 °C for 30 min (a) without NaOH and (b) mixed with 10 wt% NaOH.

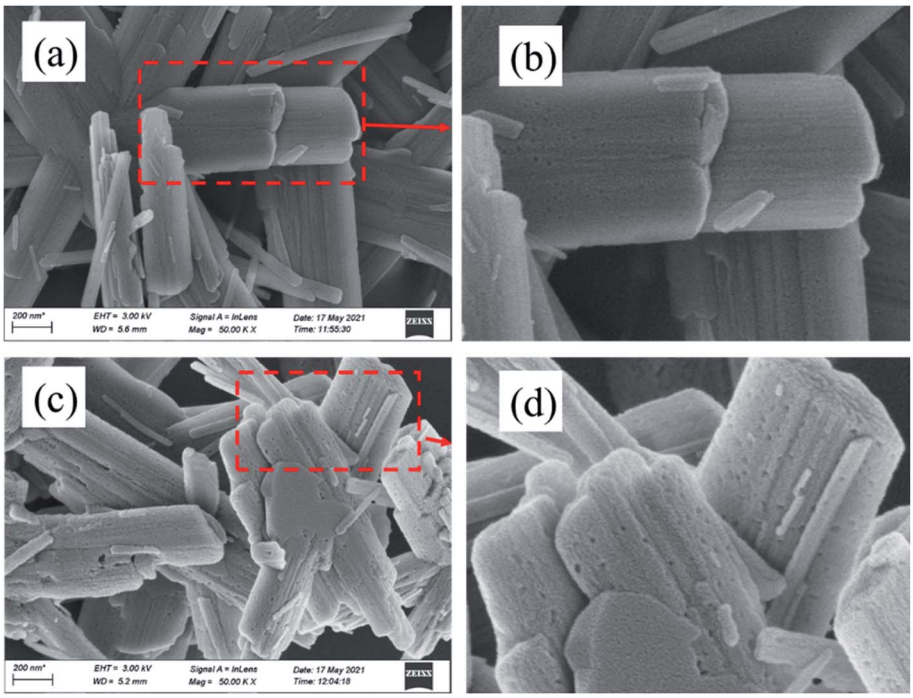

Fig. 8 SEM images of the roasted products of synthetic Al-goethite at 360 °C for 30 min (a) and (b) without NaOH and (c) and (d) mixed with 10 wt% NaOH.

goethite and Al-goethite.[39] The last one occurred at temperatures ranging from 410 °C to 564 °C, and the endothermic peak at approximately 482 °C could be associated with boehmite decomposition.[42,43] The curves in Fig. 10(b) show some variations in the size of the endothermic peaks and temperatures, and the total weight loss at 820 °C was 22.47%. The endothermic peak at different stages appeared at temperatures 196 °C, 289 °C, 347 °C, and 470 °C. The endothermic peak in the first stage at 196 °C is related to the generation of sodium aluminate.[44] Compared without the addition of NaOH, the temperature of the endothermic peaks of gibbsite, goethite/Al-goethite, and boehmite on the DSC curve with NaOH decreased by 13 °C, 17 °C, and 12 °C, respectively, implying that NaOH is

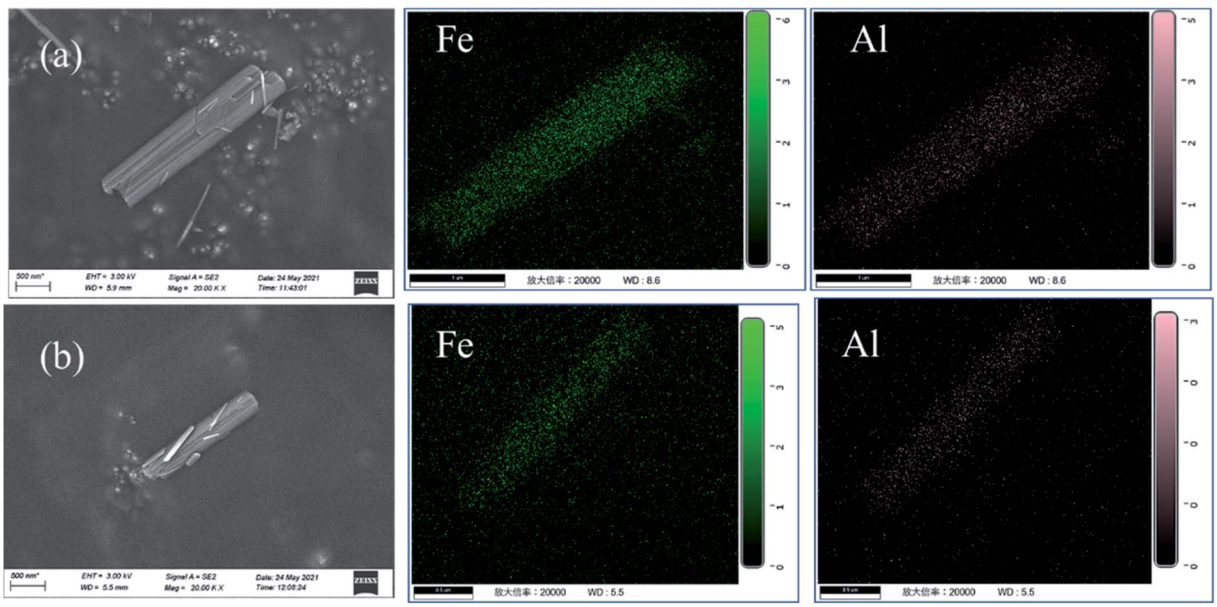

Fig. 9 SEM images and Fe, Al-mapping of the roasted products of synthetic Al-goethite at 360 °C for 30 min (a) without NaOH and (b) mixed with 10 wt% NaOH.

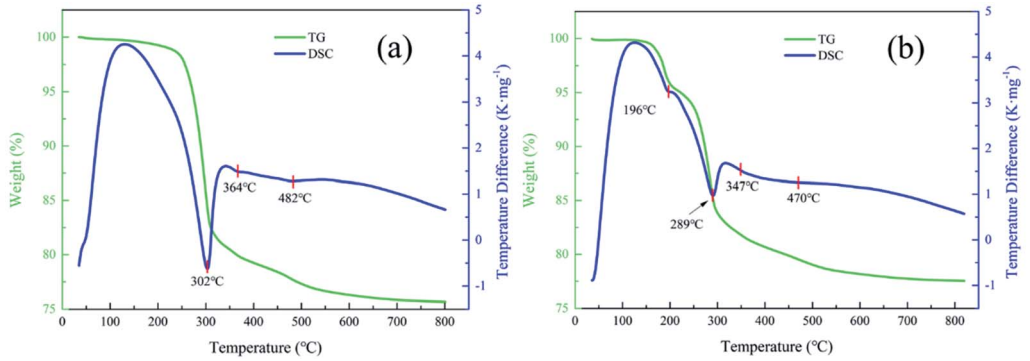

Fig. 10 TG–DSC curves of gibbsitic bauxite (a) without NaOH and (b) mixed with 10 wt% NaOH.

beneficial to decreasing the transition temperature of gibbsite, goethite/Al-goethite, and boehmite.

3.3.2 Loss on ignition. To determine the change in mass percentage of water resulting from the conversion of gibbsitic bauxite, loss on ignition was performed. The effect of the roasting temperature between 200 °C and 400 °C on the weight loss of gibbsitic bauxite without NaOH and mixed with 10 wt% NaOH was investigated, and the related weight losses are displayed in Fig. 11. The mass loss of gibbsitic bauxite without NaOH or gibbsitic bauxite mixed with 10 wt% NaOH increased with the temperature. The mass loss of gibbsitic bauxite with the addition of NaOH reached 10.26% at 240 °C, which was higher than the 2.71% mass loss of gibbsitic bauxite without NaOH, indicating that the addition of NaOH can accelerate the mass loss of gibbsitic bauxite. Combined with TG–DSC in Fig. 10(b), the reason for this phenomenon is the reaction of NaOH and gibbsite.

3.3.3 XRD analysis. To further comprehend the phase conversion of gibbsitic bauxite during low-temperature roasting, the XRD patterns of roasted gibbsitic bauxite mixed without NaOH and mixed with 10 wt% NaOH over temperatures ranging from 200 °C to 400 °C for 30 min are displayed in Fig. 12. Fig. 12(a) shows that the gibbsite and Al-goethite present in the raw bauxite disappeared during roasting, and the diffraction intensities of the characteristic boehmite and hematite peaks were slightly enhanced, indicating that gibbsite and Al-goethite underwent phase conversions as a result of heating, changing to boehmite and hematite, respectively, through the loss of moisture. The quartz, rutile, and anatase are stable phases and do not undergo a phase transition below 400 °C, thus showing no significant change in the diffraction peak related to quartz, rutile, and anatase. As is shown in Fig. 12(b), the XRD patterns are similar to the process of roasting gibbsitic bauxite in the case of adding NaOH, but the temperature at which the diffraction peak of Al-goethite disappears is reduced from 400 °C to 360 °C compared to the process without adding NaOH, implying that NaOH is beneficial to promoting the conversion of Al-goethite. Compared with roasting gibbsitic bauxite alone above 320 °C, gibbsite remained (probably trapped by the newly generated sodium aluminate) when the temperature was raised to 400 °C.

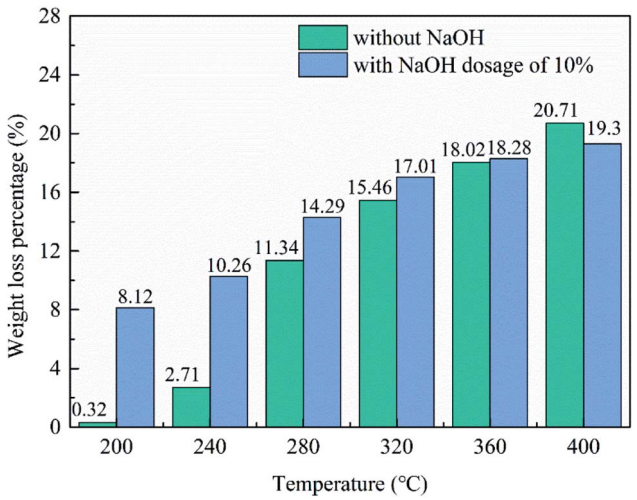

Fig. 11 Effect of roasting temperature on weight loss of gibbsitic bauxite.

3.3.4 SEM analysis. To further understand the microscopic conversion of Al-goethite and gibbsite/boehmite in gibbsitic bauxite during low-temperature roasting, the SEM, and EDS mapping for initial gibbsitic bauxite, and roasted one at 400 °C for 30 min were investigated and displayed in Fig. 13. The SEM and EDS in Fig. 13 show that gibbsite/boehmite appear gray–black, while Al-goethite is bright-gray. Compared with initial gibbsitic bauxite, the gibbsite/boehmite and Al-goethite in gibbsitic bauxite after roasting at 400 °C for 30 min appear more pores due to the dehydrogenation. It can be speculated that the substituted Al in goethite can contact the Bayer liquor, favoring the increase of the relative alumina recovery during Bayer digestion.

3.4 Effect of thermal conversion gibbsitic bauxite in Bayer digestion

3.4.1 Alumina recovery. To minimize the inhibitory effect caused by Al-goethite on gibbsitic bauxite digestion, the low-temperature roasting process was used to pretreat bauxite before Bayer digestion. Fig. 14 shows the relative alumina recovery derived from the typical high-temperature Bayer

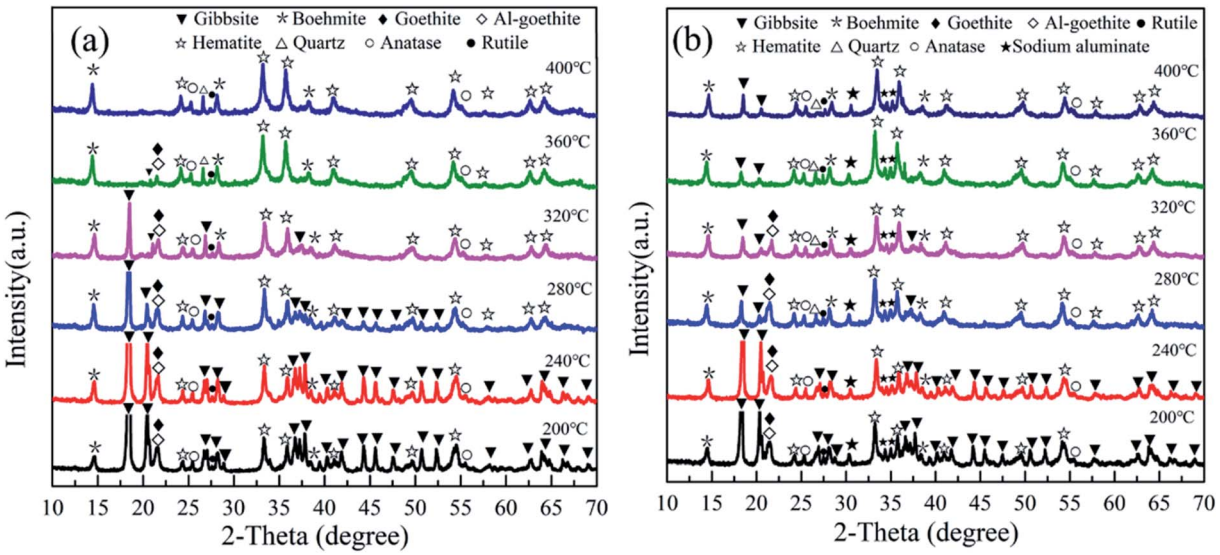

Fig. 12 XRD patterns of roasted products of gibbsitic bauxite at 200–400 °C for 30 min (a) without NaOH and (b) mixed with 10 wt% NaOH.

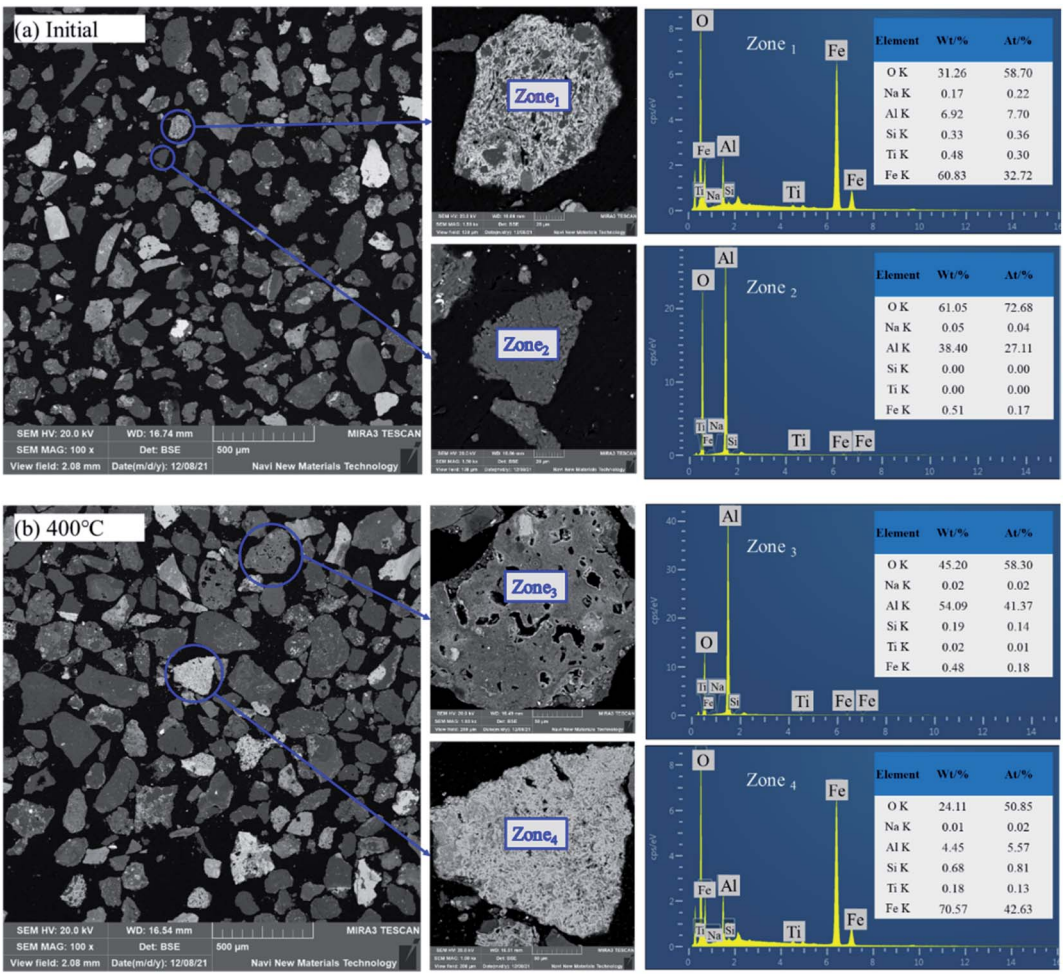

Fig. 13 Characterization of the SEM morphology, and EDS mapping with (a) initial gibbsitic bauxite, and (b) roasted one at 400 °C for 30 min.

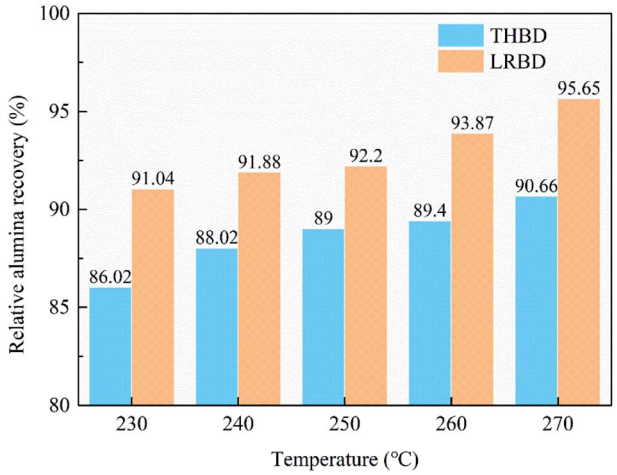

Fig. 14 Effects of temperature on relative alumina recovery of typical Bayer digestion and low-temperature roasting-Bayer digestion (t = 60 min, 100 mL Bayer liquid, 31.25 g bauxite or 24.78 g roasted bauxite at 400 °C for 30 min [weight loss rate of 79.24% based on LOI analysis]).

digestion (THBD, direct Bayer digestion) and low-temperature roasting-Bayer digestion (LRBD, roasted bauxite at 400 °C for 30 min followed by Bayer digestion). Fig. 14 shows that the relative alumina recovery from THBD at 230 °C for 60 min was only 86.02%, indicating that substantial Al-goethite is present in the red mud. As the temperature continues to increase to 270 °C, the relative alumina recovery only increased to 90.66%, which is consistent with the poor digestion performance of Al-goethite containing gibbsitic bauxite in the industry. However, the relative alumina recovery in LRBD varied from 91.04% to 95.65%, indicating that the alumina recovery was approximately 5% higher than the one in THBD at the same conditions because dense Al-goethite in gibbsitic bauxite has been transformed into a porous Al-hematite, which are beneficial to the interaction of aluminum in Al-hematite and Bayer liquor.

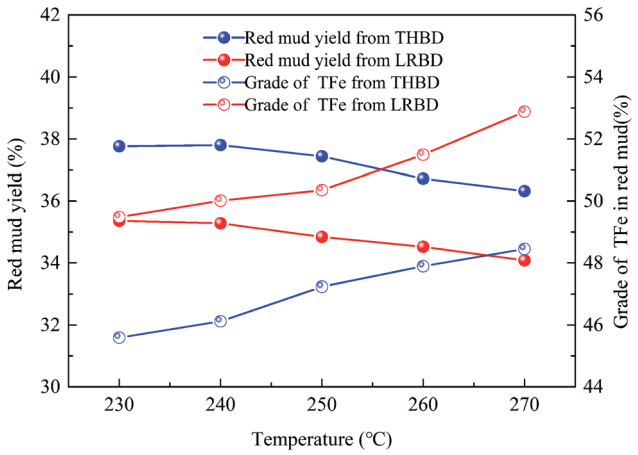

Fig. 15 Influence of digestion temperature on yield of red mud and grade of TFe in red mud (t = 60 min, 100 mL Bayer liquid, 31.25 g bauxite or 24.78 g roasted bauxite at 400 °C for 30 min [weight loss rate of 79.24% based on LOI analysis]).

3.4.2 Enrichment of iron. Efficient gibbsitic bauxite digestion is conducive to the decrease of solid waste generation and the enrichment of iron minerals in red mud. The grade of TFe in the red mud produced from the THBD and LRBD is shown in Fig. 15. Fig. 15 shows that the yield of the red mud from THBD decreased from 37.76% to 36.32%, and thus the grade of TFe in the red mud increased from 45.59% to 48.45% with the change of the digestion temperature between 230 °C and 270 °C. Nevertheless, the yield of red mud from LRBD decreased from 35.36% to 34.08% and the grade of TFe in the red mud from the LRBD varied from 49.48% to 52.88% as the temperature increased from 230 °C to 270 °C. This result shows that the yield of red mud and the grade of TFe was approximately 4% higher and 2.5%, respectively, compared with the red muds from the THBD at the same conditions, indicating that the conversion of Al-goethite to Al-hematite in gibbsitic bauxite was beneficial to decreasing the yield of red mud and increasing the grade of TFe in red mud, which are conducive to the enrichment and utilization of iron minerals.

3.4.3 Remove of TOC. The low-temperature roasting process may decompose organic compounds in bauxite, thus decreasing organic content in Bayer liquid during Bayer digestion process. The changes in the organic content of the Bayer liquid during digestion before and after low-temperature roasting bauxite were studied and the results are presented in Fig. 16. From Fig. 16, it is worth noting that the TOC concentration of the typical Bayer liquor varied between 347.4 mg L^{-1} and 425.8 mg L^{-1}, while that of the Bayer liquor from LRBD varied between 64.1 mg L^{-1} and 70.1 mg L^{-1} when the digestion temperature varied between 230 °C and 270 °C. The results show the organic matter content in the Bayer liquor decreased by 67.4% during the Bayer process, indicating that some organic matter in bauxite can be removed by roasting at 400 °C for 30 min. According to the literature, organic matter may be oxalic acid, humic acids, cellulose, and humus.[45–47]

3.4.4 XRD and SEM analysis. To further investigate the effects of temperature on minerals conversion during the

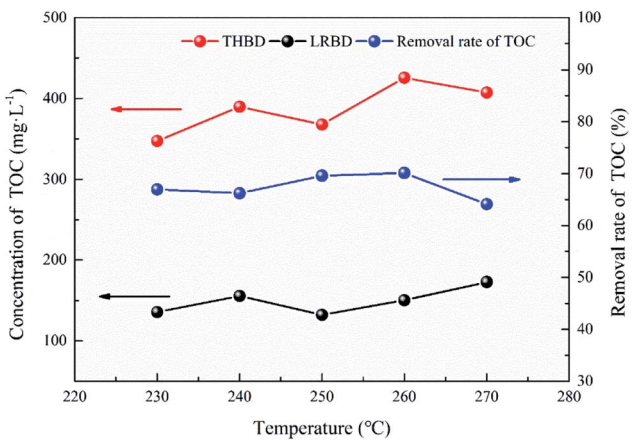

Fig. 16 Influence of digestion temperature on TOC in digestion liquor (t = 60 min, 100 mL Bayer liquid, 31.25 g bauxite or 24.78 g roasted bauxite at 400 °C for 30 min [weight loss rate of 79.24% based on LOI analysis]).

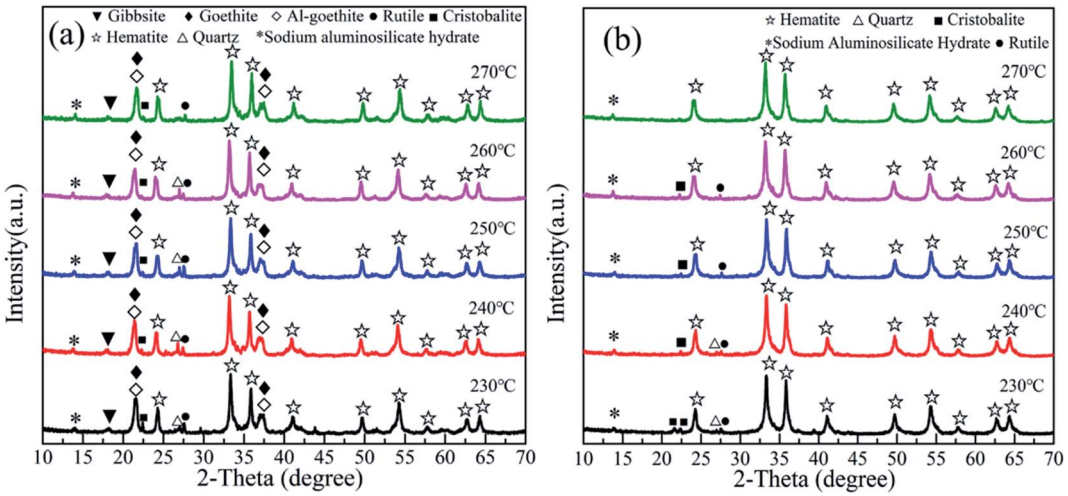

Fig. 17 Influence of digestion temperature on minerals phase transition during (a) THBD and (b) LRBD (t = 60 min, 100 mL Bayer liquid, 31.25 g bauxite or 24.78 g roasted bauxite at 400 °C for 30 min [weight loss rate of 79.24% based on LOI analysis]).

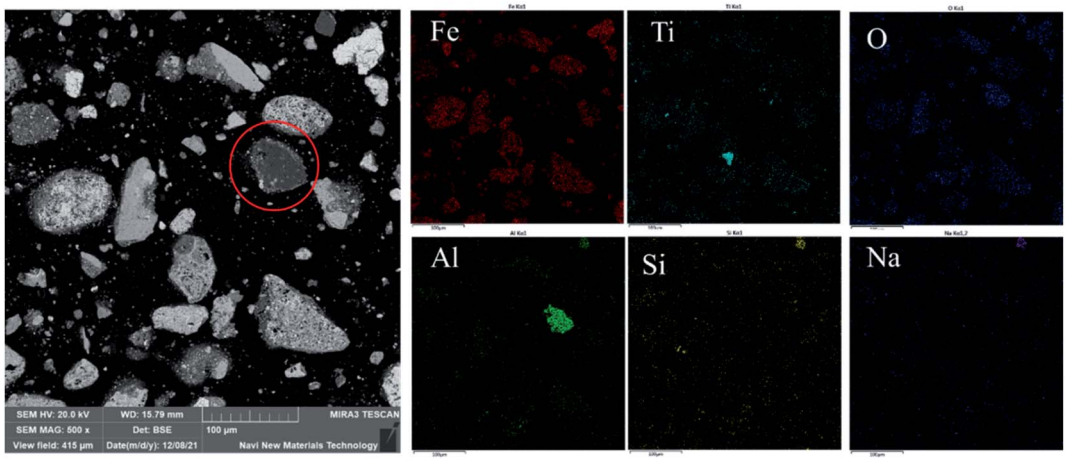

Fig. 18 The SEM morphology, and EDS mapping scanning images of red mud (T = 270 °C, t = 60 min, 31.25 g bauxite, 100 mL Bayer liquid).

digestion process, the red mud samples were characterized by XRD and SEM, and the results are presented in Fig. 17 and 18. From Fig. 17(a), the characteristic peaks of sodium aluminosilicate hydrate were observed and the intensity of the diffraction peak increases gradually with temperature rises, revealing that the higher temperatures favor sodium aluminosilicate hydrate formation. A small amount of gibbsite remained in the red mud from THBD even at 270 °C. The SEM and EDS mapping of the red mud from THBD even at 270 °C is shown in Fig. 18 and this indicates the coincidental distribution of Al, Fe, and O, which combined with the XRD pattern in Fig. 17(a), highlights the presence of Al-goethite have been blocked by the Al-goethite wrapped around the surface of the gibbsite during the Bayer digestion process. The iron-bearing minerals in red mud were mainly hematite, goethite, and Al-goethite, and the diffraction peak intensity of goethite and Al-goethite gradually weakened as the temperature increased, implying the more aluminum in Al-goethite is digested, which is consistent with the results in Fig. 14. In addition, no significant change in the diffraction peak related to quartz and rutile was observed when the temperature was below 260 °C. As the temperature rises to 270 °C, the diffraction peak intensity of quartz disappears and the rutile remained. However, it can be observed from Fig. 17(b) that the mineral compositions of red mud from LRBD were greatly simplified. The main phase was hematite and minor minerals were quartz, cristobalite, and rutile. Compared with THBD, the diffraction peak intensity of the minor minerals in red mud from LRBD disappeared at a lower temperature, implying that LRBD is more conducive to the reaction of minor minerals with the Bayer liquid.

4. Conclusions

(1) The goethite and Al-goethite in Guinea gibbsitic bauxite account for approximately 5.05% and 15.90%, respectively, and the latter's aluminum content proportion is as high as 12.68%,

which exists in the form of irregular, plate-like, or long strip granules. Portions of goethite and Al-goethite cover the surface of the gibbsite particles in the form of aggregates.

(2) The conversion temperature of synthetic Al-goethite starts at a rather low temperature, ~280 °C, while that of natural Al-goethite starts at ~320 °C. We could attribute this difference in conversion temperature to the shielding effect of the admixtures, such as gibbsite, quartz, and hematite, in bauxite. The roasting process experiences a phase change from Al-goethite to Al-hematite without any morphological change in the original Al-goethite-like appearance, which has many pores due to de-hydroxylation.

(3) Low-temperature roasting Bayer process can improve the thermal conversion of Al-goethite to hematite and remove a certain amount of organic matter in gibbsitic bauxite, increasing the relative digestion ratio of alumina and the grade of TFe in red mud by approximately 6% and 4%, respectively, and decreasing the yield of red mud and the content of organic matter in the Bayer liquor by about 6% and 67%, respectively.

Author contributions

Guotao Zhou: investigation, experimental, formal analysis and writing–original draft. Yilin Wang: funding acquisition, conceptualization, methodology, review and editing. Tiangui Qi: review and editing. Qiusheng Zhou: review and editing. Guihua Liu: review and editing. Zhihong Peng: review and editing. Xiaobin Li: conceptualization, review and editing.

Conflicts of interest

There are no conflicts to declare.

Acknowledgements

This work was financially supported by the National Natural Science Foundation of China [grant number 52104353].

References

1 International Aluminium Institute, 2020, https://www.world-aluminium.org.
2 A. R. Hind, S. K. Bhargava and S. C. Grocott, *Colloids Surf., A*, 1999, **146**, 359–374.
3 F. Feret, M. Authier-Martin and I. Sajo, *Clays Clay Miner.*, 1997, **45**, 418–427.
4 P. G. Fazey, B. H. O'Connor and L. C. Hammond, *Clays Clay Miner.*, 1991, **39**, 248–253.
5 D. G. Schulze, *Clays Clay Miner.*, 1984, **32**, 36–44.
6 N. Brown and R. J. Tremblay, *Light Met.*, 1974, **3**, 825–844.
7 D. Lawson, A. Rijkeboer, D. Dajkovich, M. Jackson and H. Lawrence, *Light Met.*, 2014, 11–18.
8 K. Solymar, I. Sajo, J. Steiner and J. Zoldi, *Light Met.*, 1992, 209–223.
9 J. Murray, L. Kirwan, M. Loan and B. K. Hodnett, *Hydrometallurgy*, 2009, **95**, 239–246.
10 X. L. Pan, H. Y. Yu, K. W. Dong, G. F. Tu and S. W. Bi, *Int. J. Miner., Metall. Mater.*, 2012, **19**, 973–977.
11 B. I. Whittington, *Hydrometallurgy*, 1996, **43**, 13–35.
12 B. Xu, P. Smith, C. Wingate and L. D. Silva, *Hydrometallurgy*, 2010, **105**, 75–81.
13 H. Arkan, G. K. Demir and S. Vural, *Int. J. Ind. Chem.*, 2019, **10**, 57–66.
14 B. I. Whittington, *Hydrometallurgy*, 1996, **43**, 13–35.
15 S. G. Xue, F. Zhu, X. F. Kong, C. Wu, L. Huang, N. Huang and W. Hartley, *Environ. Sci. Pollut. Res.*, 2016, **23**, 1120–1132.
16 G. Power, M. Gräfe and C. Klauber, *Hydrometallurgy*, 2011, **108**, 33–45.
17 L. Y. Li, *Waste Manag.*, 2001, **21**, 525–534.
18 X. B. Li, L. L. Kong, T. G. Qi, Q. S. Zhou, Z. H. Peng and G. H. Liu, *Chin. J. of Nonferrous Met.*, 2013, **23**, 544–548.
19 X. B. Li, Z. Y. Zhou, Y. L. Wang, Q. S. Zhou, T. G. Qi, G. H. Liu and Z. H. Peng, *Trans. Nonferrous Met. Soc. China*, 2020, **30**, 1980–1990.
20 L. Diamandescu, D. Mihàilà-Tàràbàşanu and M. Feder, *Mater. Lett.*, 1993, **17**, 309–311.
21 E. Wolska, W. Szajda and P. Piszora, *Solid State Ionics*, 1994, **70**, 537–541.
22 H. D. Ruan, R. L. Frost, J. T. Kloprogge and L. Duong, *Spectrochim. Acta, Part A*, 2002, **58**, 479–491.
23 E. Wolska, W. Szajda and P. Piszora, *J. Therm. Anal.*, 1992, **38**, 2115–2122.
24 U. Schwertmann, *Thermochim. Acta*, 1984, **78**, 39–46.
25 C. A. Barrero, R. E. Vandenberghe, E. D. Grave, A. L. Morales and G. Pérez, *Hyperfine Interact.*, 2003, **148**, 337–344.
26 P. S. R. Prasad, K. Shiva Prasad, V. Krishna Chaitanya, E. V. S. S. K. Babu, B. Sreedharc and S. Ramana Murthy, *J. Asian Earth Sci.*, 2006, **27**, 503–511.
27 E. Wolska, *Solid State Ionics*, 1988, **28**, 1349–1351.
28 R. L. Frost, Z. Ding and H. D. Ruan, *J. Therm. Anal. Calorim.*, 2003, **71**, 783–797.
29 G. González, A. Sagarzazu and R. Villalba, *Mater. Res. Bull.*, 2000, **35**, 2295–2308.
30 V. Nunna, S. Hapugoda, M. I. Pownceby and G. J. Sparrow, *Miner. Eng.*, 2021, **166**, 106826.
31 Y. Zhang, Q. Gao, J. Zhao, M. Li and Y. Qi, *Minerals*, 2019, **9**, 223.
32 V. P. Ponomar, *Miner. Eng.*, 2018, **127**, 143–152.
33 V. Ravisankar, R. Venugopal and H. Bhat, *Miner. Process. Extr. Metall.*, 2019, **128**, 175–182.
34 K. O. Jang, V. R. M. Nunna, S. Hapugoda, A. V. Nguyen and W. J. Bruckard, *Miner. Eng.*, 2014, **60**, 14–22.
35 N. O. Dudchenko and V. P. Ponomar, *Vìsnik Dnìpropetrovs'kogo Unìversitetu: Serìâ Geologìâ*, 2015, **23**, 25–32.
36 T. Hiemstra, J. C. M. D. Wit and W. H. V. Riemsdijk, *J. Colloid Interface Sci.*, 1989, **133**, 105–117.
37 M. L. Li, H. B. Liu, T. H. Chen, L. Wei, C. Wang, W. Hu and H. L. Wang, *Chem. Geol.*, 2019, **524**, 368–382.
38 H. Wang, Z. Zhang, K. Arnon, J. Chen and W. Han, *Trans. Chin. Soc. Agric. Eng.*, 2018, **34**, 124–131.
39 R. Derie, M. Ghodsi and C. Calvo-Roche, *J. Therm. Anal.*, 1976, **9**, 435–440.

40 Y. Mochizuki and N. Tsubouchi, *ACS Omega*, 2019, **4**, 19723–19734.
41 V. J. Ingram-Jones, R. Slade, T. W. Davies and S. Salvador, *J. Mater. Chem.*, 1996, **6**, 73.
42 A. Atasoy, *J. Therm. Anal. Calorim.*, 2007, **90**, 153–158.
43 C. Z. Liao, L. Zeng and K. Shih, *Chemosphere*, 2015, **131**, 171–177.
44 S. J. Kim, J. I. Lee, K. S. Han, S. Y. Byun, T. Tran and M. J. Kim, *Korean J. Met. Mater.*, 2018, **56**, 49–58.
45 M. A. Wellington, *Ind. Eng. Chem. Res.*, 2013, **52**, 2013.
46 K. Rao and R. Goyal, *Light Met.*, 2006, 71–74.
47 G. Power, *Hydrometallurgy*, 2010, **105**, 1–29.